Nonlinear dynamics of Mathieu resonators for resonant gyroscope applications

Najib Kacem, S. Hentz, Sébastien Baguet, Régis Dufour

Nonlinear dynamics of Mathieu resonators for resonant gyroscope applications

Dynamique non linéaire des résonateurs de Mathieu pour les applications de gyromètres résonants

Najib Kacem[13], Sébastien Hentz[2], Sébastien Baguet[3] and Régis Dufour[3]

[1]Microsystems Components Laboratory

CEA/LETI /3DSI/DIHS/LCMS, 17 rue des Martyrs 38054 Grenoble, France

Tel: +33-4-38-78-01-27; Fax: +33-4-38-78-24-34; E-mail: najib.kacem@cea.fr

[2]Device simulation and characterization Laboratory

CEA/LETI /3DSI/D2NT/LSCDP, 17 rue des Martyrs 38054 Grenoble, France

Tel: +33-4-38-78-28-91; Fax: +33-4-38-78-45-83; E-mail: sebastien.hentz@cea.fr

[3]LaMCoS, INSA-Lyon, CNRS-UMR5259, 569621, France

18, Rue des Sciences Bâtiment d'Alembert 69621 Villeurbanne, France

Tel: +33-4-72-43-81-93; Fax: +33-4-78-89-09-80; E-mail: Sebastien.Baguet@insa-lyon.fr

Tel: +33-4-72-43-82-02; Fax: +33-4-72-43-89-30; E-mail: regis.dufour@insa-lyon.fr

ABSTRACT

Operation at resonance is not only advantageous for micromechanical actuators but also for sensing. The sensor is comprised of elements that operate at their characteristic resonance and the effect of the measurand is detected as a change in the resonant characteristics of these elements. Resonant sensing often involves the detection of an input measurand by means of a resonant frequency shift in the sensing device.

The resonant sensing technique [1] is highly sensitive, has the potential for large dynamic range, good linearity, low noise and potentially low power. However, when scaling sensors down to NEMS, nonlinearities occur sooner [2] restricting the benefits of the resonant sensors. Moreover, for resonant gyroscopes, the frequency of the Coriolis forces becomes closer to the resonator frequency. The idea is to investigate the dynamic behaviour of nonlinear Mathieu resonator [3] in order to find the optimal physical conditions for gyroscope designers to maximise the sensors performances.

Keywords: MEMS \ gyroscope \ Mathieu resonator \ non linear dynamics \ dynamic range

RESUME

Travailler à la résonance n'est pas seulement avantageux en actuation micromécanique mais aussi en détection. Un capteur à détection fréquentielle comprend un élément sensible résonant qui oscille à sa fréquence propre. L'effet de la mesurande modifie cette fréquence de résonance, souvent avec une loi quasi linéaire qui s'étend sur une gamme de mesure identifiable. Le paramètre physique à mesurer est détecté sous forme d'un décalage fréquentiel.

Le mode de détection fréquentielle [1] a pour avantages d'être extrêmement sensible, a le potentiel d'avoir une large gamme dynamique, peu sensible au bruit, une large gamme de linéarité et une faible consommation électrique. Cependant, en réduisant la taille des détecteurs vers les NEMS, les non-linéarités apparaissent rapidement [2] limitant ainsi les avantages des capteurs fréquentiels. De plus, pour les gyromètres résonnants, la fréquence des forces de Coriolis devient comparable à la fréquence du résonateur. L'idée est d'examiner le comportement dynamique des résonateurs non linéaire de Mathieu [3] afin de trouver les conditions physiques optimales pour les concepteurs de gyroscope dans le but de maximiser les performances de ce type de capteur.

Mots clés: MEMS \ gyromètre \ résonateur de Mathieu \ dynamique non linéaire \ gamme dynamique

1 Introduction

The permanent quest for cost cuts has led to the use of potential "In-IC" compatible thin SOI-based technologies, which imposes drastic size reduction of the sensors. Combined with the need for in-plane actuation for fabrication and design simplicity, this implies a large reduction in detectability. Moreover nonlinearities [4] occur sooner for small structures which reduce their dynamic range.

In the context of a "small" z-axis resonant gyroscope (Figure 1) designed with high actuation frequency, the dynamic of the sensing part governed by a nonlinear Mathieu equation has been modelled.

The device consists of a proof mass suspended by flexures attached to a rigid frame. The proof mass is driven relative to the outer frame using embedded lateral comb drive actuators. If an external rotation θ is applied to the chip about the z-axis, the Coriolis force $F_c = 2M\theta V$ acting on the proof mass is transmitted to the outer frame and communicated axially onto two resonators.

The periodic compression and tension of the resonators by the Coriolis force at the proof mass drive frequency modulates the resonant frequency of these force sensors. Each resonator embedded in the feedback loop of an oscillator circuit. Thus, by demodulating the oscillation frequency, the rotation rate applied to the device can be estimated.

The Mathieu equation has been widely studied in the context of parametric resonance, but our study will be restricted to the primary resonance on the way of design optimisation for high drive frequencies in order to enhance the dynamic range of resonant micro-gyroscopes.

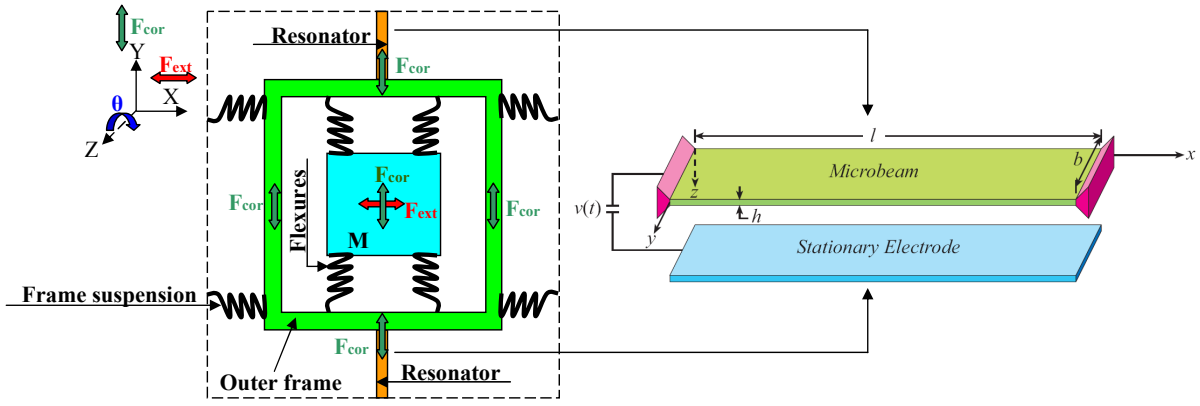

FIG. 1 – Schema of the resonant microgyroscope

2 Device and equations

The resonant output gyroscope [5] shown in figure (1), as its name implies, utilizes resonant sensing as the basis for Coriolis force detection. In its simplest form, the device consists of three resonating elements, a proof mass and two resonating sense elements.

2.1 Equation of motion

The dynamics of the device can be described by series of coupled differential equations. The proof mass dynamics can be described for most part by a classical spring-mass-damper equation. The dynamics of the resonators subjected to an axial time-varying Coriolis force is described by a nonlinear partial differential equation. The respective equations can be written as :

$$\frac{d^2X(\tilde{t})}{d\tilde{t}^2} + \frac{\tilde{\delta}}{Q}\frac{dX(\tilde{t})}{d\tilde{t}} + \tilde{\delta}^2 X(\tilde{t}) = \frac{F_e}{M}\cos\tilde{\delta}\tilde{t} \tag{1}$$

$$EI\frac{\partial^4\tilde{w}(\tilde{x},\tilde{t})}{\partial\tilde{x}^4} + \rho bh\frac{\partial^2\tilde{w}(\tilde{x},\tilde{t})}{\partial\tilde{t}^2} + \tilde{c}\frac{\partial\tilde{w}(\tilde{x},\tilde{t})}{\partial\tilde{t}} =$$

$$\left[\tilde{N} + \tilde{F}_c\cos\tilde{\delta}\tilde{t} + \frac{Ebh}{2l}\int_0^l\left[\frac{\partial\tilde{w}(\tilde{x},\tilde{t})}{\partial\tilde{x}}\right]^2 d\tilde{x}\right]\frac{\partial^2\tilde{w}(\tilde{x},\tilde{t})}{\partial\tilde{x}^2} \tag{2}$$

$$+\frac{1}{2}\varepsilon_0\frac{bC_n\left[Vdc + Vac\cos(\tilde{\Omega}\tilde{t})\right]^2}{(g-\tilde{w}(\tilde{x},\tilde{t}))^2}$$

$$\tilde{w}(0,\tilde{t}) = \tilde{w}(l,\tilde{t}) = \frac{\partial\tilde{w}}{\partial\tilde{x}}(0,\tilde{t}) = \frac{\partial\tilde{w}}{\partial\tilde{x}}(l,\tilde{t}) = 0 \tag{3}$$

where X is the proof mass displacement along the drive axis, Q is the drive quality factor, δ and F_e are the drive angular frequency and the electrostatic drive force applied to the proof mass M. $\tilde{x}$ is the position along the microbeam length, E and I are the Young's modulus and moment of inertia of the cross section. $\tilde{N}$ is the applied tensile axial force due to the residual stress on the silicon or the effect of the measurand, $\tilde{t}$ is the time, ρ is the material density, h is the microbeam thickness, g is the capacitor gap width, and ε_0 is the dielectric constant of the gap medium. The last term in equation (2) represents an approximation of the electric force assuming a complete overlap of the area of the microbeam and the stationary electrode including the edge effects by the coefficient C_n.

2.2 Normalization

For convenience and equations simplicity , we introduce the nondimensional variables :

$$w = \frac{\tilde{w}}{g}, \;\; x = \frac{\tilde{x}}{l}, \;\; t = \frac{\tilde{t}}{\tau} \tag{4}$$

Where $\tau = \frac{2l^2}{h}\sqrt{\frac{3\rho}{E}}$. Substituting equation (4) into equations (2) and (3), we obtain :

$$\begin{aligned} &\frac{\partial^4 w}{\partial x^4} + \frac{\partial^2 w}{\partial t^2} + c\frac{\partial w}{\partial t} - \alpha_2 \frac{\left[Vdc + Vac\cos(\Omega t)\right]^2}{(1-w))^2} \\ &= \left[N + F_c \cos\delta t + \alpha_1 \int_0^1 \left[\frac{\partial w}{\partial x}\right]^2 dx\right] \frac{\partial^2 w}{\partial x^2} \\ &w(0,t) = w(1,t) = \frac{\partial w}{\partial x}(0,t) = \frac{\partial w}{\partial x}(1,t) = 0 \end{aligned} \tag{5}$$

The parameters appearing in equations (5) are :

$$\begin{aligned} &c = \frac{\tilde{c}l^4}{EI\tau}, \;\; N = \frac{\tilde{N}l^2}{EI}, \;\; F_c = \frac{\tilde{F}_c l^2}{EI}, \;\; \delta = \tilde{\delta}\tau \\ &\alpha_1 = 6\left[\frac{g}{h}\right]^2, \;\; \alpha_2 = 6\frac{\varepsilon_0 l^4}{Eh^3 g^3}, \;\; \Omega = \tilde{\Omega}\tau \end{aligned} \tag{6}$$

2.3 Resolution

A reduced-order model is generated by modal decomposition transforming equations (5) into a finite-degree-of-freedom system consisting of ordinary differential equations in time. We use the undamped linear mode shapes of the straight microbeam as basis functions in the Galerkin procedure. To this end, we express the deflection as :

$$w(x,t) = \sum_{k=1}^{n} a_k(t)\phi_k(x) \tag{7}$$

Where $a_k(t)$ is the k^{th} generalized coordinate and $\phi_k(x)$ is the k^{th} linear undamped mode shape of the straight microbeam, normalized such that $\int_0^1 \phi_k \phi_j = 0$ for $k \neq p$ and governed by :

$$\frac{d^4\phi_k(x)}{dx^4} = \lambda_k^2 \phi_k(x) \tag{8}$$

$$\phi_k(0) = \phi_k(1) = \phi_k'(0) = \phi_k'(1) \tag{9}$$

Here, λ_k is the k^{th} natural frequency of the microbeam. We multiply equations (5) by $\phi_k(x)(1-w)^2$, substitute equations (7) into the resulting equation, use equations (8) to eliminate $\dfrac{d^4\phi_k(x)}{dx^4}$, integrate the outcome from $x=0$ to 1, and obtain :

$$\begin{aligned}
&\ddot{a}_k + c_k\dot{a}_k + \lambda_k^2 a_k \\
&-2\sum_{j=1}^{n}\left\{\lambda_j^2 {a_j}^2 + c_j a_j \dot{a}_j + a_j \ddot{a}_j\right\}\int_0^1 \phi_k {\phi_j}^2 dx \\
&+\sum_{j=1}^{n}\left\{\lambda_j^2 {a_j}^3 + c_j {a_j}^2 \dot{a}_j + {a_j}^2 \ddot{a}_j\right\}\int_0^1 \phi_k {\phi_j}^3 dx \\
&-\sum_{j=1}^{n}\left\{\left(N + F_c\cos\delta t\right)a_j + \alpha_1 {a_j}^3\int_0^1\left[\phi_j'\right]^2 dx\right\}\int_0^1 \phi_k\phi_j'' dx \\
&+2\sum_{j=1}^{n}\left\{\alpha_1 {a_j}^4\int_0^1\left[\phi_j'\right]^2 dx + \left(N + F_c\cos\delta t\right){a_j}^2\right\}\int_0^1 \phi_k\phi_j\phi_j'' dx \\
&-\sum_{j=1}^{n}\left\{\alpha_1 {a_j}^5\int_0^1\left[\phi_j'\right]^2 dx + \left(N + F_c\cos\delta t\right){a_j}^3\right\}\int_0^1 \phi_k {\phi_j}^2\phi_j'' dx \\
&= \alpha_2\left[Vdc + Vac\cos(\Omega t)\right]^2\int_0^1 \phi_k dx
\end{aligned} \tag{10}$$

Noting that the first mode should be the dominant mode of the system and the other modes are neglected, so it is sufficient to consider the case $n=1$. Equation (10) becomes :

$$\begin{aligned}
&\ddot{a}_1 + (500.564 + 12.3\left(N + F_c\cos\delta t\right))a_1 + (1330.9 + 38.3\left(N + F_c\cos\delta t\right)){a_1}^2 \\
&+\left(927 + 28\left(N + F_c\cos\delta t\right) + 151\alpha_1\right){a_1}^3 + 471\alpha_1 {a_1}^4 + 347\alpha_1 {a_1}^5 \\
&+c_1\dot{a}_1 + 2.66c_1 a_1\dot{a}_1 + 1.85c_1{a_1}^2\dot{a}_1 + 2.66a_1\ddot{a}_1 \\
&+1.85{a_1}^2\ddot{a}_1 = -\frac{8}{3\pi}\alpha_2\left[Vdc + Vac\cos(\Omega t)\right]^2
\end{aligned} \tag{11}$$

To analyse the equation of motion (11), it is convenient to invoke perturbation techniques [5] which work well with the assumptions of "small" excitation and damping, typically valid in MEMS resonators.

In order to facilitate the perturbation approach using the method of averaging, a standard constrained coordinate transformation is introduced, as given by :

$$\begin{cases} a_1 = A(t)\cos\left[\Omega t + \beta(t)\right] \\ \dot{a}_1 = -A(t)\Omega\sin\left[\Omega t + \beta(t)\right] \\ \ddot{a}_1 = -A(t)\Omega^2\cos\left[\Omega t + \beta(t)\right] \end{cases} \tag{12}$$

In addition, since near-resonant behavior is the principal operating regime of the proposed system, a detuning parameter, σ is introduced, as given by :

$$\Omega = \omega_n + \varepsilon\sigma \tag{13}$$

Separating the resulting equations and averaging them over the period $\frac{2\pi}{\Omega}$ in the t-domain results in the system's averaged equations, in terms of amplitude and phase, which are given by :

$$\begin{aligned} \frac{\dot{A}}{\varepsilon} = &-\frac{Ac_1}{2} - 0.23A^3c_1 - \frac{7A^3\cos[4\beta]F_c}{8\pi\left(\delta - 4\omega_n\right)} + \frac{7A^3\cos\left[4\beta - \frac{2\pi\delta}{\omega_n}\right]F_c}{8\pi\left(\delta - 4\omega_n\right)} - \frac{0.76A^2\cos[3\beta]F_c}{\delta - 3\omega_n} \\ &+\frac{0.76A^2\cos\left[3\beta - \frac{2\pi\delta}{\omega_n}\right]F_c}{\delta - 3\omega_n} - \frac{0.5A\cos[2\beta]F_c}{\delta - 2\omega_n} + \frac{7A^3\sin\left[2\beta - \frac{\pi\delta}{\omega_n}\right]\sin\left[\frac{\pi\delta}{\omega_n}\right]F_c}{2\pi\left(\delta - 2\omega_n\right)} \\ &+\frac{0.5A\cos\left[2\beta - \frac{2\pi\delta}{\omega_n}\right]F_c}{\delta - 2\omega_n} - \frac{0.76A^2\cos[\beta]F_c}{\delta - \omega_n} + \frac{0.76A^2\cos\left[\beta + \pi\left(2 - \frac{2\delta}{\omega_n}\right)\right]F_c}{\delta - \omega_n} \\ &+\frac{8\mathrm{VacVdc}\sin[\beta]\alpha_2}{3\pi\omega_n} + \frac{0.76A^2\cos[\beta]F_c}{\delta + \omega_n} - \frac{0.76A^2\cos\left[\beta + \frac{2\pi(\delta+\omega_n)}{\omega_n}\right]F_c}{\delta + \omega_n} \\ &+\frac{0.5A\cos[2\beta]F_c}{\delta + 2\omega_n} + \frac{7A^3\cos[2\beta]F_c}{4\pi\left(\delta + 2\omega_n\right)} - \frac{0.5A\cos\left[2\left(\beta + \pi\left(2 + \frac{\delta}{\omega_n}\right)\right)\right]F_c}{\delta + 2\omega_n} \\ &-\frac{7A^3\cos\left[2\left(\beta + \pi\left(2 + \frac{\delta}{\omega_n}\right)\right)\right]F_c}{4\pi\left(\delta + 2\omega_n\right)} + \frac{0.76A^2\cos[3\beta]F_c}{\delta + 3\omega_n} + \frac{7A^3\cos[4\beta]F_c}{8\pi\left(\delta + 4\omega_n\right)} \\ &-\frac{7A^3\cos\left[4\beta + 2\pi\left(4 + \frac{\delta}{\omega_n}\right)\right]F_c}{8\pi\left(\delta + 4\omega_n\right)} - \frac{0.76A^2\cos\left[3\beta + 2\pi\left(3 + \frac{\delta}{\omega_n}\right)\right]F_c}{\delta + 3\omega_n} \end{aligned} \tag{14}$$

$$\frac{\dot{\beta}}{\varepsilon} = -\frac{0.98\sin\left[\frac{2\pi\delta}{\omega_n}\right]F_c}{\delta} + 0.7A^2\omega_n + \mathrm{A}\sigma - \frac{7A^2\sin[4\beta]F_c}{8\pi\left(\delta - 4\omega_n\right)} + \frac{7A^2\sin\left[4\beta + \pi\left(8 - \frac{2\delta}{\omega_n}\right)\right]F_c}{8\pi\left(\delta - 4\omega_n\right)}$$

$$+\frac{0.76A\sin\left[3\beta + \pi\left(6 - \frac{2\delta}{\omega_n}\right)\right]F_c}{\delta - 3\omega_n} - \frac{9A^2\cos[\beta]\sin[\beta]F_c\omega_n}{\delta^2 - 4\omega_n^2} - \frac{4.6A\sin[3\beta]F_c\omega_n}{\delta^2 - 9\omega_n^2}$$

$$+\frac{2.3A\sin\left[\beta + \pi\left(2 - \frac{2\delta}{\omega_n}\right)\right]F_c}{\delta - \omega_n} - \frac{347.6A^2}{\omega_n} - \frac{10.5A^2N}{\omega_n} - \frac{56.6A^2\alpha_1}{\omega_n} - \frac{108.4A^4\alpha_1}{\omega_n}$$

$$-\frac{0.85\mathrm{VacVdc}\cos[\beta]\alpha_2}{A\omega_n} - \frac{2.3A\sin\left[\beta + \frac{2\pi(\delta+\omega_n)}{\omega_n}\right]F_c}{\delta + \omega_n} - \frac{4.6A\sin[\beta]F_c\omega_n}{\delta^2 - \omega_n^2} \tag{15}$$

$$-\frac{7A^2\sin\left[2\left(\beta + \pi\left(2 + \frac{\delta}{\omega_n}\right)\right)\right]F_c}{2\pi\left(\delta + 2\omega_n\right)} - \frac{0.76A\sin\left[3\beta + 2\pi\left(3 + \frac{\delta}{\omega_n}\right)\right]F_c}{\delta + 3\omega_n} + \frac{7A^2\sin[4\beta]F_c}{8\pi\left(\delta + 4\omega_n\right)}$$

$$-\frac{7A^2\sin\left[4\beta + 2\pi\left(4 + \frac{\delta}{\omega_n}\right)\right]F_c}{8\pi\left(\delta + 4\omega_n\right)} - \frac{21A^2\sin\left[\frac{2\pi\delta}{\omega_n}\right]F_c}{4\pi\delta} + \frac{7A^2\sin\left[2\beta + \pi\left(4 - \frac{2\delta}{\omega_n}\right)\right]F_c}{2\pi\left(\delta - 2\omega_n\right)}$$

$$-\frac{4\cos[\beta]\sin[\beta]F_c\omega_n}{\delta^2 - 4\omega_n^2} - \frac{0.5\sin\left[2\left(\beta + \pi\left(2 + \frac{\delta}{\omega_n}\right)\right)\right]F_c}{\delta + 2\omega_n} + \frac{0.5\sin\left[2\beta + \pi\left(4 - \frac{2\delta}{\omega_n}\right)\right]F_c}{\delta - 2\omega_n}$$

The steady-state motions occur when $\dot{A} = \dot{\beta} = 0$, which corresponds to the singular points of the equations system (14) and (15). Thus, the frequency-response equation can be writen in its parametric form as :

$$\begin{cases} \sigma = f[\beta, \delta] \\ \\ A = f[\beta, \delta] \end{cases} \tag{16}$$

3 Results

The effect of the Coriolis force frequency in the resonator frequency response at its primary resonance is shown in Figure (2). The ratio between the drive and the resonator frequency varies from 0.25 to 1 and the external rotation applied to the device about the z-axis is about $150^{\circ}/s$. We observe the separation of the curve branches when the Coriolis frequency equals the resonator frequency.

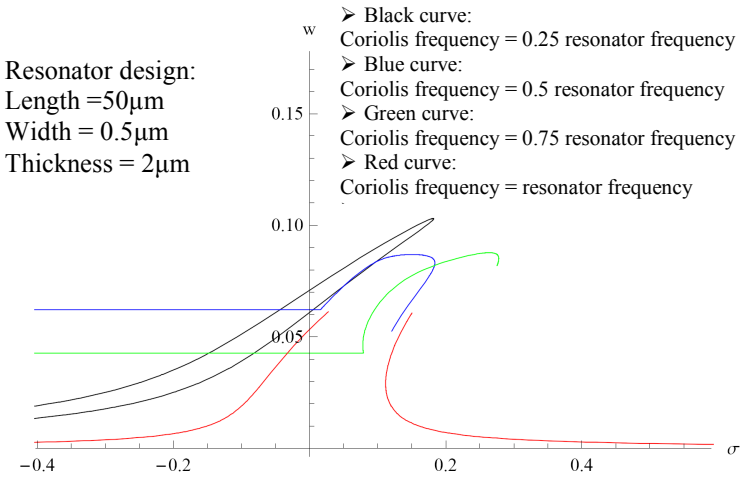

FIG. 2 – Predicted forced frequency responses.

The particular case of a ratio between the drive frequency and the resonator frequency equal to 1 is treated in Figure (3) for different kinds of resonator behavior. The gap between the stable and the unstable branches appears for w exceeds w_p and pull-in develops. w_p depends on the physic parameters of the resonator and the angular rate θ.

It appears also that the quality factor decreases when the external rotation applied to the microgyroscope increases. For detection stability, embedding the resonators in the feedback loop of an oscillator circuit [5] permits the conservation of a uniform sensitivity through a defined full scale limited by a critical amplitude.

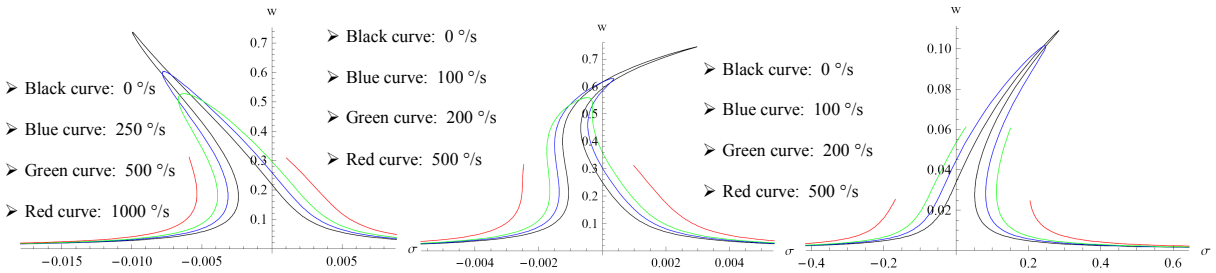

Fig.3.a: Softening behavior | Fig.3.b: Mixed behavior | Fig.3.c: Hardening behavior

Resonator design: length =100µm, width = 5µm, thickness = 2µm.	Resonator design: length =50µm, width = 0.5µm, thickness = 2µm.

FIG. 3 – Predicted forced frequency responses for different angular rates of the resonant microgyrosope.

Figure (4) shows the effect of the parametric and the nonlinear terms in the periodicity of the resonator response and its amplitude(length $=50\mu m$, width $= 0.5\mu m$, thickness $= 2\mu m$). Moreover, the transition to the quasi-periodicity is shown in the phase plane when the drive frequency equals the resonator frequency and for an external rotation $\theta = 1000^{\circ}/s$. This phenomenon is due to the resonator frequency modulation by the parametric terms but it can be also a consequence of the energy transfer between the parametric terms in the Mathieu equation and the nonlinear Vander pool damping term [6]. The quasi-periodicity of the resonator response may lead to a chaotic [3] device.

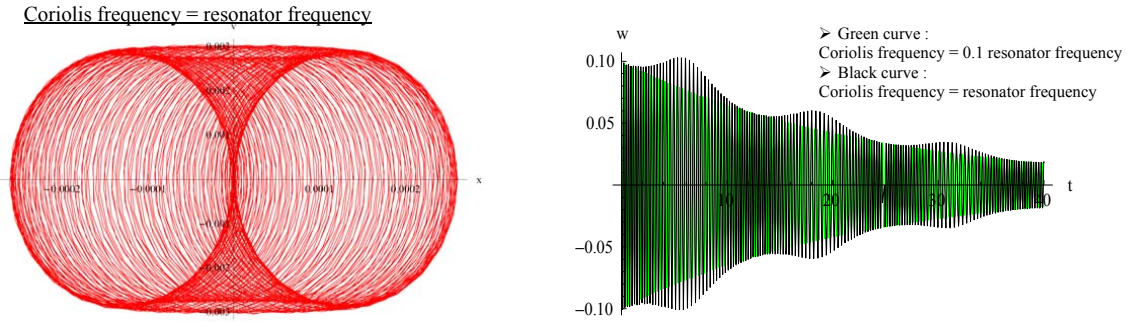

Fig.4.a: Phase plane

Fig.4.b: Time history

FIG. 4 – Long time integration

Another limitation for the full scale of a resonant microgyroscope is underlined : the frequency ratio between the proof mass actuation and the resonator sensing. It appears in Figure (5) that the symmetry can be broken between negative and positive Coriolis stress effect when the resonator is losing the stability for high coriolis forces amplitude and frequency. The maximum of displacement is situated at 0.6 of the frequency ratio.

4 Conclusions

A complete analytical model describing the nonlinear dynamics of Mathieu resonators applied to resonant MEM gyroscopes has been presented. The model is based on the Galerkin discretization coupled with a perturbation technique (the averaging method) enabling the study of the dynamic behaviour of the sensing parts of these devices. In addition, this model constitutes a quick and powerful tool on the way of understanding the different dynamics phenomena and the description of the dynamics transition from periodicity to quasi-periodicity.

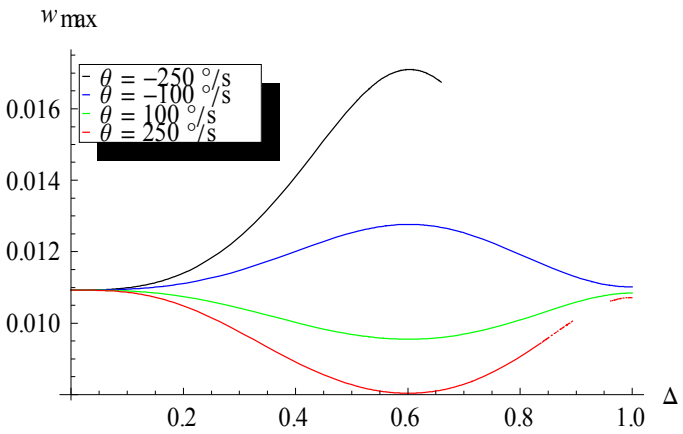

FIG. 5 – Variation of $Wmax$ with the frequency ratio between the drive and the sense

In this paper, it proves that increasing the drive frequency of the proof mass for resonant microgyroscopes can be advantageous in order to increase the detectability of the device (the maximum is situated at 0.6 of frequency ratio between the drive part and the sense part). This improvement has a direct effect on the full scale of the microgyroscope which will be limited by the instability of the Mathieu resonator.

REFERENCES

[1] T. Roessig, "IntegratedMEMStuning fork oscillators for sensor applications," Ph.D. dissertation, Department of Mechanical Engineering, University of California, Berkeley, 1998.

[2] Gui, C., Legrenberg, R., Tilmans, H.A., Fluitman, J.H.J., Elwenspoek, M. : "Nonlinearity and hysteresis of resonant strain gauges", J. Microelectromech. Syst. 7, 122-127 (1998).

[3] Barry E. DeMartini, Holly E. Butterfield,, Jeff Moehlis, and Kimberly L. Turner, Member, "Chaos for a Microelectromechanical Oscillator Governed by the Nonlinear Mathieu Equation", J. Microelectromech. Syst., Vol. 16, No. 6, December 2007.

[4] N.Kacem, S.Hentz, H.Fontaine, V.Nguyen, P.Robert, B.Legrand and L.Buchaillot, "From MEMS to NEMS : Modelling and characterization of the non linear dynamics of resonators, a way to enhance the dynamic range," Nanotech 2008 (Boston).

[5] Seshia, A.A.; Howe, R.T.; Montague, S, "An integrated microelectromechanical resonant output gyroscope," Technical Digest Fifteenth IEEE International Conference on Micro Electro Mechanical Systems (MEMS 2002), Las Vegas, NV, p.722-726.

[6] Nayfeh, A.H. : Introduction to Perturbation Techniques. Wiley, New York (1981).

[7] Mohamed Belhaq and Abdelhak Fahsi, "frequency locking in fast excited van der Pol Mathieu Duffing oscillator," Nonlinear Dyn. (2007).